

Multiple Instance Active Learning for Object Detection

Tianning Yuan[†], Fang Wan[†], Mengying Fu[†],
Jianzhuang Liu[†], Songcen Xu[†], Xiangyang Ji[§] and Qixiang Ye^{†*}

[†]University of Chinese Academy of Sciences, Beijing, China

[†]Noah’s Ark Lab, Huawei Technologies, Shenzhen, China. [§]Tsinghua University, Beijing, China

{yuantianning19, fumengying19}@mails.ucas.ac.cn, {wanfang, qxye}@ucas.ac.cn

{liu.jianzhuang, xusongcen}@huawei.com, xyji@tsinghua.edu.cn

Abstract

Despite the substantial progress of active learning for image recognition, there still lacks an instance-level active learning method specified for object detection. In this paper, we propose Multiple Instance Active Learning (MIAL), to select the most informative images for detector training by observing instance-level uncertainty. MIAL defines an instance uncertainty learning module, which leverages the discrepancy of two adversarial instance classifiers trained on the labeled set to predict instance uncertainty of the unlabeled set. MIAL treats unlabeled images as instance bags and feature anchors in images as instances, and estimates the image uncertainty by re-weighting instances in a multiple instance learning (MIL) fashion. Iterative instance uncertainty learning and re-weighting facilitate suppressing noisy instances, toward bridging the gap between instance uncertainty and image-level uncertainty. Experiments validate that MIAL sets a solid baseline for instance-level active learning. On commonly used object detection datasets, MIAL outperforms state-of-the-art methods with significant margins, particularly when the labeled sets are small. Code is available at <https://github.com/yuantn/MIAL>.

1. Introduction

The key idea behind active learning is that a machine learning algorithm can achieve better performance with fewer training samples if it is allowed to select the data it wants to learn from. Despite the rapid progress of learning methods with less supervision [21, 20], e.g., weakly supervised learning and semi-supervised learning, active learning

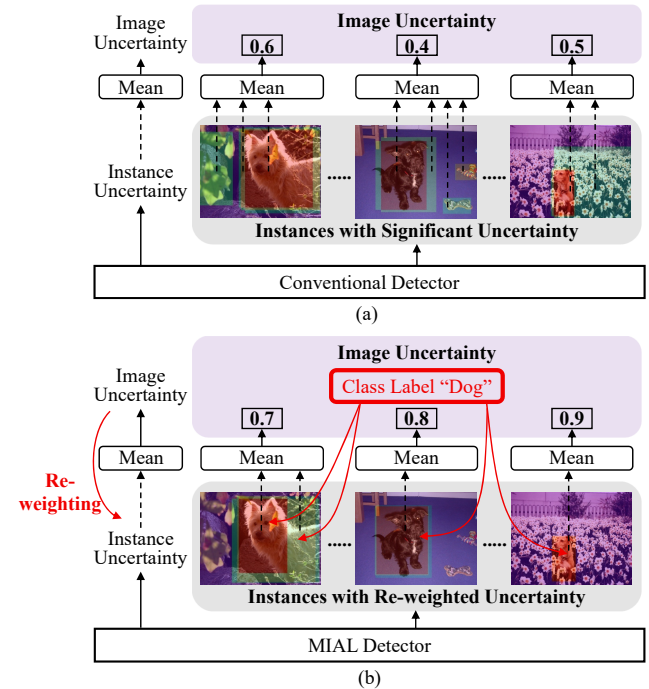


Figure 1. Comparison of active object detection methods. (a) Conventional methods compute image uncertainty by simply averaging instance uncertainties, ignoring interference from a large number of background instances. (b) Our MIAL approach leverages uncertainty re-weighting via multiple instance learning to filter out interfering instances while bridging the gap between instance uncertainty and image uncertainty. (Best viewed in color)

remains the cornerstone of many practical applications for its simplicity and higher performance bound.

In the computer vision area, active learning has been widely explored for image classification (active image classification) by empirically generalizing the model trained on the labeled sets to the unlabeled sets [9, 30, 18, 37, 4, 24, 36,

*Corresponding Author.

[\[25, 34\]](#). Uncertainty-based methods define various metrics for selecting informative images and adapting trained models to the unlabeled set [\[9\]](#). Distribution-based approaches [\[30, 1\]](#) aim at estimating the layout of unlabeled images to select samples of large diversity. Expected model change methods [\[8, 15\]](#) find out samples that can cause the greatest change of model parameters or the largest loss [\[40\]](#).

Despite the substantial progress, there still lacks an instance-level active learning method specified for object detection (active object detection). Active object detection has been defined by recent studies [\[40, 41, 2\]](#). The objective goal is to select the most informative images for detector training. However, they tackled it by simply summarizing/averaging instance/pixel uncertainty as image uncertainty and unfortunately ignored the large imbalance of negative instances in object detection, which causes significant noisy instances in the background and interferes with the learning of image uncertainty, Fig. 1(a).

In this paper, we propose a Multiple Instance Active Learning (MIAL) approach for object detection, Fig. 1(b), and target at selecting informative images from the unlabeled set by learning and re-weighting instance uncertainty with discrepancy learning and multiple instance learning (MIL). To learn the instance-level uncertainty, MIAL first defines an instance uncertainty learning (IUL) module, which leverages two adversarial instance classifiers plugged atop the detection network (*e.g.*, a feature pyramid network) to learn the uncertainty of unlabeled instances. Maximizing the prediction discrepancy of two instance classifiers predicts instance uncertainty while minimizing classifiers' discrepancy drives learning features to reduce the distribution bias between labeled and unlabeled instances.

To establish the relationship between instance uncertainty and image uncertainty, MIAL incorporates a MIL module, which is in parallel with the instance classifiers. MIL treats each unlabeled image as an instance bag and performs instance uncertainty re-weighting (IUR) by evaluating instance appearance consistency across images. During MIL, the instance uncertainty and image uncertainty are forced to be consistently driven by a classification loss defined on image class labels (or pseudo-labels). Optimizing the image-level classification loss facilitates suppressing the noisy instances while highlighting truly representative ones. Iterative instance uncertainty learning and instance uncertainty re-weighting bridge the gap between instance-level observation and image-level evaluation, towards selecting the most informative images for detector training.

The contributions of this paper include:

(1) We propose Multiple Instance Active Learning (MIAL), establishing a solid baseline to model the relationship between the instance uncertainty and image uncertainty for informative image selection.

(2) We design instance uncertainty learning (IUL) and

instance uncertainty re-weighting (IUR) modules, providing effective approaches to highlight informative instances while filtering out noisy ones in object detection.

(3) We apply MIAL to object detection on commonly used datasets, improving state-of-the-art methods with significant margins.

2. Related Work

2.1. Active Learning

Active learning, as one of the most important research topics in machine learning, has attracted intensive attention in the past few years. In the computer vision area, active learning methods are mostly proposed for image classification, which can be roughly categorized into uncertainty-based and distribution-based.

Uncertainty-based Methods. Uncertainty is the most popular metric to select samples for active learning [\[31\]](#), which can be defined as the posterior probability of a predicted class [\[17, 16\]](#), or the margin between the posterior probabilities of the first and the second predicted class [\[14, 28\]](#). It can also be defined upon entropy [\[32, 26, 14\]](#), which measures the variance of unlabeled samples. The expected model change methods [\[29, 33\]](#) utilized the present model to estimate the expected network gradient or expected prediction changes [\[8, 15\]](#), which guide the sample selection. MIL-based methods [\[33, 13, 38, 6\]](#) selected informative images by discovering representative instances. However, these methods are designed for image classification and are not applicable to object detection due to the challenging aspect of the crowded and noisy instances.

Distribution-based Methods. This line of methods selects diverse and informative samples by estimating the distribution of unlabeled samples. Clustering methods [\[27\]](#) were applied to build the unlabeled sample distribution while discrete optimization methods [\[11, 7, 39\]](#) were employed to perform sample selection. By considering the distances to their surrounding samples, the context-aware methods [\[12, 3\]](#) selected the samples that can represent the global sample distribution. Core-set [\[30\]](#) defined the problem of active learning as core-set selection, *i.e.*, choosing a set of points such that a model learned on the labeled subset captures the diversity of the unlabeled samples.

In the deep learning era, active learning methods remain falling into the uncertainty-based or distribution-based routines [\[18, 37, 4\]](#). Sophisticated methods have extended active learning to the open sets [\[24\]](#), or combined it with self-paced learning [\[36\]](#). Nevertheless, it remains questionable whether or not the intermediate feature representation is effective for sample selection. The learning loss approach [\[40\]](#) can be categorized as either uncertainty-based or distribution-based. By introducing a network structure to predict the “loss” of the unlabeled samples, it estimates

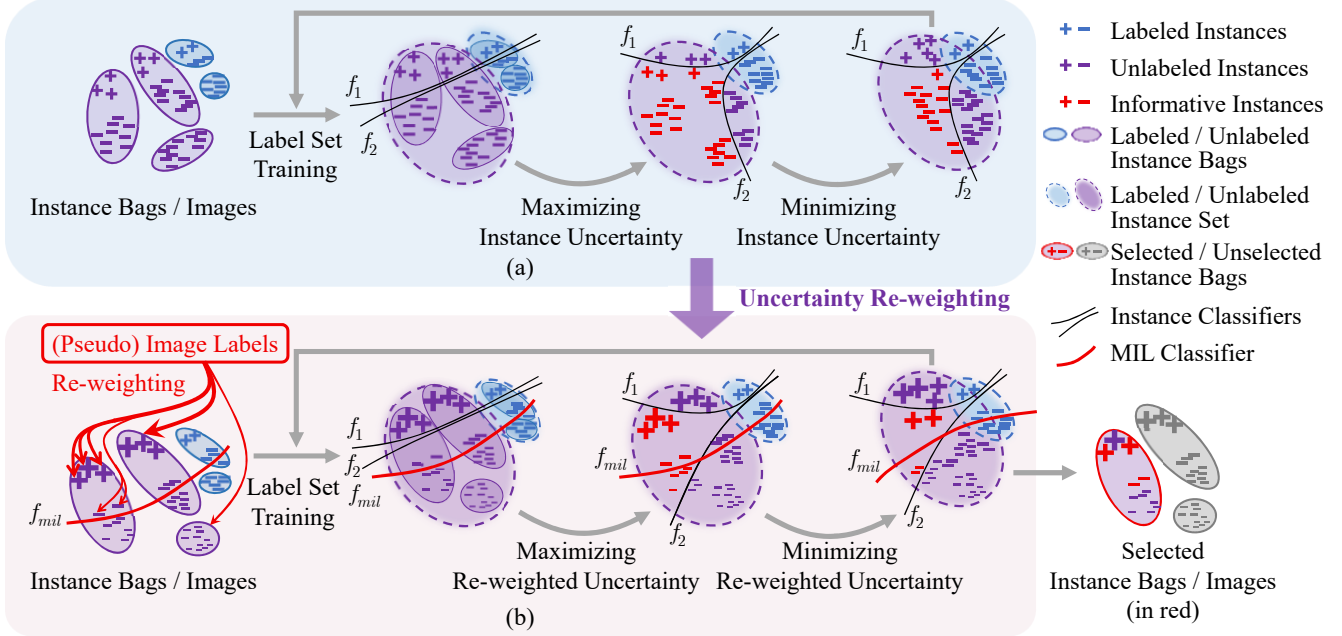


Figure 2. MIAL illustration. (a) Instance uncertainty learning (IUL) utilizing two adversarial classifiers. (b) Instance uncertainty re-weighting (IUR) using multiple instance learning. Bigger symbols (“+” and “-”) indicate larger weights. (Best viewed in color)

sample uncertainty and distribution, and selects samples with large “loss” like hard negative mining.

2.2. Active Learning for Object Detection

Despite the substantial progress of active learning, few methods were specified for active object detection, which faces complex instance distributions in the same images and thereby is far more challenging than active image classification. By simply sorting the loss predictions of instances to evaluate the image uncertainty, the learning loss method [40] specified for image classification was directly applied to object detection. In [2], the image-level uncertainty was estimated by the uncertainty of a large number of background pixels. The CDAL approach [1] introduced spatial context to active detection and selected diverse samples according to their distances to the labeled set. Existing approaches simply used instance/pixel-level observations to represent the image-level uncertainty. There still lacks a systematic method to learn the image uncertainty by leveraging instance-level models (*e.g.*, object detectors).

3. The Proposed Approach

3.1. Overview

For active object detection, a small set of images \mathcal{X}_L^0 (the labeled set) with instance labels \mathcal{Y}_L^0 and a large set of images \mathcal{X}_U^0 (the unlabeled set) without labels are given. For each image, the label consists of bounding boxes (y_x^{loc}) and categories (y_x^{cls}) for objects of interest. A detection model

M_0 is firstly initialized by using the labeled set $\{\mathcal{X}_L^0, \mathcal{Y}_L^0\}$. With the initialized model M_0 , active learning targets at selecting a set of images \mathcal{X}_S^0 from \mathcal{X}_U^0 to be manually labeled and merging them with \mathcal{X}_L^0 to form the new labeled set \mathcal{X}_L^1 , *i.e.*, $\mathcal{X}_L^1 = \mathcal{X}_L^0 \cup \mathcal{X}_S^0$. The selected image set \mathcal{X}_S^0 should be the most informative, *i.e.*, can improve the detection performance as much as possible. Based on the updated labeled set \mathcal{X}_L^1 , the task model is retrained and updated to M_1 . The detection model training and sample selection procedures repeat several cycles until the number of labeled images reaches the annotation budget.

Considering the large number¹ of instances in each image, there are two key problems for active object detection: (1) how to evaluate the uncertainty of the unlabeled instances using the detector trained on the labeled set; (2) how to precisely estimate the image uncertainty while filtering out noisy instances. MIAL handles these two problems by introducing two learning modules respectively. For the first problem, MIAL incorporates instance uncertainty learning, with the aim of highlighting informative instances in the unlabeled set, as well as aligning the distributions of the labeled and unlabeled set, Fig. 2(a). It is motivated by the fact that most active learning methods remain simply generalizing the models trained on the labeled set to the unlabeled set. This is problematic when there is a distribution bias between the two sets [10]. For the second problem, MIAL introduces MIL to both the labeled and unlabeled set

¹For example, the RetinaNet detector [19] produces ~100k of anchors (instances) for an image.

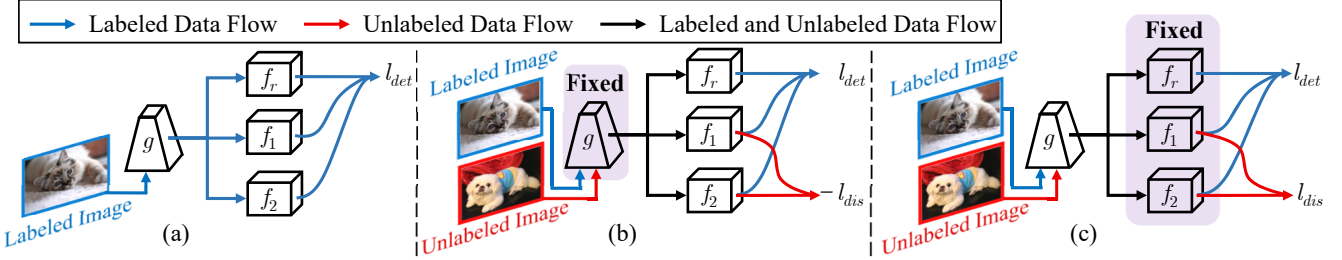


Figure 3. Network architecture for instance uncertainty learning. (a) Label set training. (b) Maximizing instance uncertainty by maximizing classifier prediction discrepancy. (c) Minimizing instance uncertainty by minimizing classifier prediction discrepancy.

to estimate the image uncertainty by re-weighting the instance uncertainty. This is done by treating each image as an instance bag while re-weighting the instance uncertainty under the supervision of the image classification loss. Optimizing the image classification loss facilitates highlighting truly representative instances belonging to the same object classes while suppressing the noisy ones, Fig. 2(b).

3.2. Instance Uncertainty Learning

Label Set Training. Using the RetinaNet as the baseline [19], we construct a detector with two discrepant instance classifiers (f_1 and f_2) and a bounding box regressor (f_r), Fig. 3(a). We utilize the prediction discrepancy between the two instance classifiers to learn the instance uncertainty on the unlabeled set. Let g denote the feature extractor parameterized by θ_g . The discrepant classifiers are parameterized by θ_{f_1} and θ_{f_2} and the regressor by θ_{f_r} . $\Theta = \{\theta_{f_1}, \theta_{f_2}, \theta_{f_r}, \theta_g\}$ denotes the set of all parameters, where θ_{f_1} and θ_{f_2} are independently initialized.

In object detection, each image x from the labeled set \mathcal{X}_L can be represented by multiple instances $\{x_i, i = 1, \dots, N\}$ corresponding to the feature anchors on the feature map [19]. N is the number of the instances in image x . $\{y_i, i = 1, \dots, N\}$ denote the labels for the instances in the image x . Given the labeled set, a detection model is trained by optimizing the following detection loss, as

$$\begin{aligned} \operatorname{argmin}_{\Theta} l_{det}(x) = \sum_i & \left(FL(\hat{y}_i^{f_1}, y_i^{cls}) + FL(\hat{y}_i^{f_2}, y_i^{cls}) \right. \\ & \left. + SmoothL1(\hat{y}_i^{f_r}, y_i^{loc}) \right), \end{aligned} \quad (1)$$

where $FL(\cdot)$ is the focal loss function for instance classification and $SmoothL1(\cdot)$ is the smooth L1 loss function for bounding-box regression [19]. $\hat{y}_i^{f_1} = f_1(g(x_i))$, $\hat{y}_i^{f_2} = f_2(g(x_i))$ and $\hat{y}_i^{f_r} = f_r(g(x_i))$ denote the prediction (classification and localization) results for the instances. y_i^{cls} and y_i^{loc} denote the ground-truth class label and bounding box label, respectively.

Maximizing Instance Uncertainty. Before the labeled set can precisely represent the unlabeled set, it is common

that there exists a distribution bias between the labeled and unlabeled set, especially when the labeled set is small. The informative instances should be localized in the biased distribution region. To find out these instances, f_1 and f_2 are designed as two adversarial instance classifiers which tend to have larger prediction discrepancy upon instances close to the class boundary, Fig. 2(a). The instance uncertainty is defined as the prediction discrepancy of f_1 and f_2 on the unlabeled set.

To find out the most informative instances, it requires to fine-tune the network and maximize the prediction discrepancy of the adversarial classifiers, Fig. 3(b). In the maximizing procedure, θ_g is fixed so that the distributions of both the labeled and unlabeled instances are fixed. θ_{f_1} and θ_{f_2} are fine-tuned on the unlabeled set to maximize the prediction discrepancies for all instances. At the same time, it requires to preserve the detection performance on the labeled set. This is fulfilled by optimizing the following loss function, as

$$\operatorname{argmin}_{\Theta \setminus \theta_g} \mathcal{L}_{max} = \sum_{x \in \mathcal{X}_L} l_{det}(x) - \sum_{x \in \mathcal{X}_U} \lambda \cdot l_{dis}(x), \quad (2)$$

where

$$l_{dis}(x) = \sum_i |\hat{y}_i^{f_1} - \hat{y}_i^{f_2}| \quad (3)$$

denotes the prediction discrepancy loss defined on the prediction discrepancy. $\hat{y}_i^{f_1}, \hat{y}_i^{f_2} \in \mathbb{R}^{1 \times C}$ are the instance classification predictions of the two classifiers for the i -th instance in image x , where C is the number of object classes in the dataset. λ is an experimentally determined regularization parameter. As shown in Fig. 2(a), the informative instances with different predictions by the adversarial classifiers tend to have larger prediction discrepancy and are assigned larger uncertainty scores.

Minimizing Instance Uncertainty. After maximizing the prediction discrepancy, we further propose to minimize the prediction discrepancy to align the distributions of the labeled and unlabeled instances, Fig. 3(c). In this procedure, the classifier parameters θ_{f_1} and θ_{f_2} are fixed, while the parameters θ_g of the feature extractor are optimized by

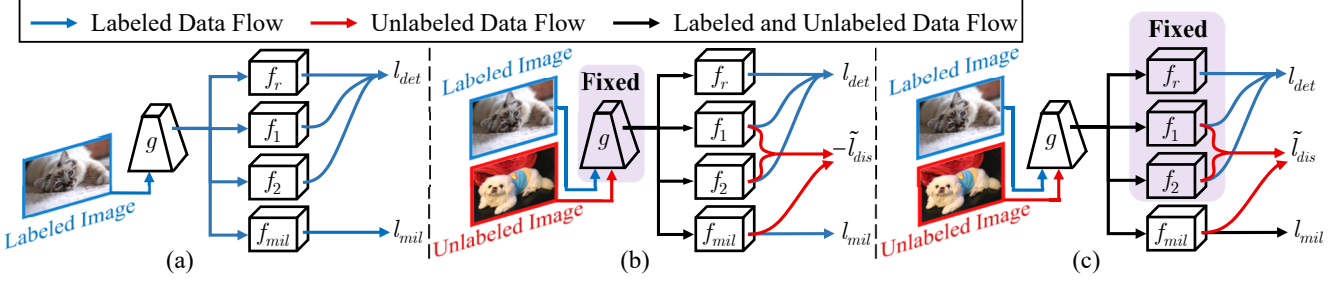


Figure 4. Network architecture for instance uncertainty re-weighting. (a) Label set training. (b) Re-weighting and maximizing instance uncertainty. (c) Re-weighting while minimizing instance uncertainty.

minimizing the prediction discrepancy loss, as

$$\operatorname{argmin}_{\theta_g} \mathcal{L}_{min} = \sum_{x \in \mathcal{X}_L} l_{det}(x) + \sum_{x \in \mathcal{X}_U} \lambda \cdot l_{dis}(x). \quad (4)$$

By minimizing the prediction discrepancy, the distribution bias between the labeled set and the unlabeled set is minimized and their features are aligned as much as possible.

In each active learning cycle, the max-min prediction discrepancy procedures repeat several times so that the instance uncertainty is learned and the instance distributions of the labeled and unlabeled set are progressively aligned. This actually defines an unsupervised learning procedure, which leverages the information (*i.e.*, prediction discrepancy) of the unlabeled set to improve the detection model.

3.3. Instance Uncertainty Re-weighting

With instance uncertainty learning, the informative instances are highlighted. However, as there is a large amount ($\sim 100k$) of instances in each image, the instance uncertainty may be not consistent with the image uncertainty. Some instances of high uncertainty are simply background noise or hard negatives for the detector. We thereby introduce an MIL procedure to bridge the gap between the instance-level and image-level uncertainty by filtering out noisy instances.

Multiple Instance Learning. MIL treats each image as an instance bag and utilizes the instance classification predictions to estimate the bag labels. In turn, it re-weights the instance uncertainty scores by minimizing the image classification loss. This actually defines an Expectation-Maximization procedure [35, 5] to re-weight instance uncertainty across bags while filtering out noisy instances.

Specifically, we add an MIL classifier f_{mil} parameterized by $\theta_{f_{mil}}$ in parallel with the instance classifiers, Fig. 4. Θ is then updated as $\tilde{\Theta} = \Theta \cup \{\theta_{f_{mil}}\}$. The MIL score $\hat{y}_{i,c}^{f_{mil}}$ for multiple instances in an image is calculated as

$$\hat{y}_{i,c}^{f_{mil}} = \frac{\exp(s_{i,c})}{\sum_c \exp(s_{i,c})} \cdot \frac{\exp((\hat{y}_{i,c}^{f_1} + \hat{y}_{i,c}^{f_2})/2)}{\sum_i \exp((\hat{y}_{i,c}^{f_1} + \hat{y}_{i,c}^{f_2})/2)}, \quad (5)$$

where $s = f_{mil}(g(x))$ is an $N \times C$ score matrix, and $s_{i,c}$ is the element in s indicating the score of the i -th instance for class c . According to Eq. (5), the MIL score $\hat{y}_{i,c}^{f_{mil}}$ is large only when x_i belongs to class c (first term in Eq. (5)) and its instance classification scores $\hat{y}_{i,c}^{f_1}$ and $\hat{y}_{i,c}^{f_2}$ are significantly larger than those of others (second term in Eq. (5)).

Considering that the MIL scores of the instances from other classes/backgrounds are small, the MIL loss l_{mil} is defined by minimizing the image classification loss using the MIL score, as

$$l_{mil}(x) = - \sum_c \left(y_c^{cls} \log \sum_i \hat{y}_{i,c}^{f_{mil}} + (1 - y_c^{cls}) \log(1 - \sum_i \hat{y}_{i,c}^{f_{mil}}) \right), \quad (6)$$

where $y_c^{cls} \in \{0, 1\}$ denotes the image class label, which can be directly obtained using the instance class label y_i^{cls} in the labeled set. Optimizing Eq. (6) drives the MIL classifier to activate instances with both large MIL score ($s_{i,c}$) and classification outputs ($\hat{y}_{i,c}^{f_1} + \hat{y}_{i,c}^{f_2}$). The instances with large classification outputs but small MIL scores ($s_{i,c}$) will be suppressed as background. The MIL loss is firstly applied in the label set training procedure to get the initial detector, and then used to re-weight the instance uncertainty in the unlabeled set.

Uncertainty Re-weighting. To ensure that the instance uncertainty is consistent with the image uncertainty, we assemble the MIL scores for all classes to a score vector w_i and re-weight the instance uncertainty as

$$\tilde{l}_{dis}(x) = \sum_i |w_i \cdot (\hat{y}_i^{f_1} - \hat{y}_i^{f_2})|, \quad (7)$$

where $w_i = \hat{y}_i^{f_{mil}}$. We then update Eq. (2) to

$$\operatorname{argmin}_{\tilde{\Theta} \setminus \theta_g} \tilde{\mathcal{L}}_{max} = \sum_{x \in \mathcal{X}_L} (l_{det}(x) + l_{mil}(x)) - \sum_{x \in \mathcal{X}_U} \lambda \cdot \tilde{l}_{dis}(x). \quad (8)$$

By optimizing Eq. (8), the discrepancies of instances with large MIL scores are preferentially estimated, while those

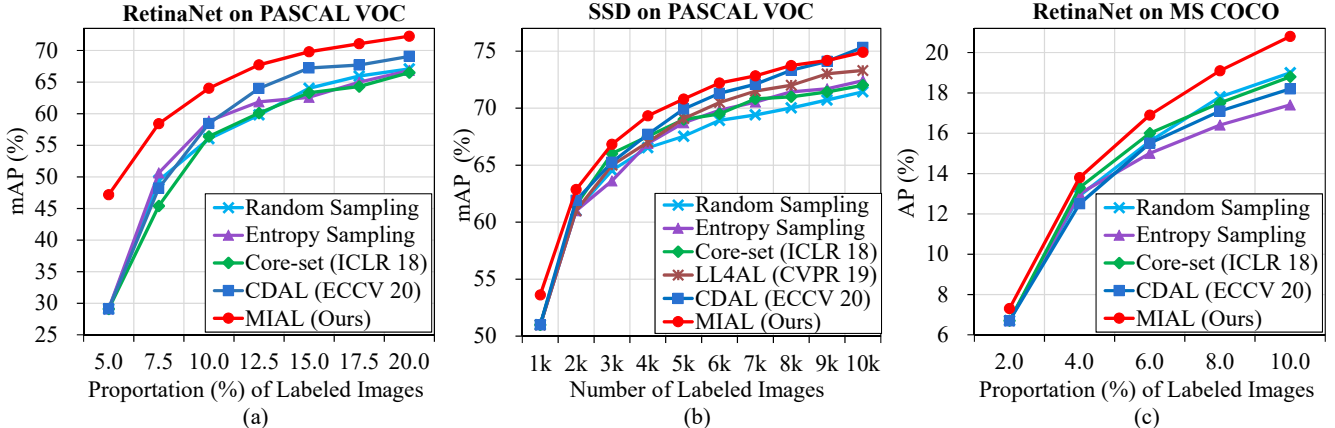


Figure 5. Performance comparison of active object detection methods. (a) On PASCAL VOC using RetinaNet backbone. (b) On PASCAL VOC using SSD backbone. (c) On MS COCO using RetinaNet backbone.

with small MIL scores are suppressed. Similarly, Eq. (4) is updated to

$$\begin{aligned} \operatorname{argmin}_{\theta_g, \theta_{f_{mil}}} \tilde{\mathcal{L}}_{min} = & \sum_{x \in \mathcal{X}_L} \left(l_{det}(x) + l_{mil}(x) \right) \\ & + \sum_{x \in \mathcal{X}_U} \left(\lambda \cdot \tilde{l}_{dis}(x) + l_{mil}(x) \right). \end{aligned} \quad (9)$$

In Eq. (9), the MIL loss is applied to the unlabeled set, where the pseudo image labels are estimated using the outputs of the instance classifiers, as

$$y_c^{pseudo} = \mathbb{1} \left(\max_i \left(\frac{\hat{y}_{i,c}^{f_1} + \hat{y}_{i,c}^{f_2}}{2} \right), 0.5 \right), \quad (10)$$

where $\mathbb{1}(a, b)$ is a binarization function. When $a > b$, it returns 1; otherwise 0. Eq. (10) is defined based on that instance classifiers can find true instances but are easy to be confused by complex backgrounds. Therefore, we use the maximum instance score to predict pseudo image labels and then leverage MIL to reduce background interference. According to Eqs. (5) and (6), the MIL loss ensures the highlighted instances are representative of the image, *i.e.*, minimizing the image classification loss so that the gap between the instance uncertainty and image uncertainty is minimized. By iteratively optimizing Eqs. (8) and (9), informative object instances with the same class are statistically highlighted, while the background instances are suppressed during the instance uncertainty learning procedure.

3.4. Informative Image Selection

In each active learning cycle, after the instance uncertainty learning (IUL) and the instance uncertainty re-weighting (IUR) procedures, we select the most informative images from the unlabeled set by observing the top- k instance uncertainty defined in Eq. (3) for each image,

where k is a hyperparameter. This is based on the fact that the noisy instances have been suppressed and the instance uncertainty has been consistent with the image uncertainty. The selected images are merged into the labeled set for the next learning cycle.

4. Experiments

In this section, we firstly introduce the experimental settings. We then report the detection performance of MIAL and compare it with state-of-the-art methods. We finally present ablation study with visualization analysis.

4.1. Experimental Settings

Datasets. The *trainval* sets of PASCAL VOC 2007 and 2012 datasets are used as the training set, which contain 5011 and 11540 images, respectively. The VOC 2007 *test* set is used to evaluate the detection performance (mean average precision (mAP)). The MS COCO dataset contains 80 object categories with challenging aspects including dense objects and small objects with occlusion. We use the *train* set with 117k images for active learning and the *val* set with 5k images for evaluating the detection performance (average precision (AP)).

Active Learning Settings. We use the RetinaNet [19] with ResNet-50 and SSD [23] with VGG-16 as the base detector. For RetinaNet, MIAL uses 5.0% of randomly selected images from the training set to initialize the labeled set on PASCAL VOC. In each active learning cycle, it selects 2.5% images from the rest unlabeled set until the labeled images reach 20.0% of the training set. For the large-scale MS COCO, MIAL uses only 2.0% of randomly selected images from the training set to initialize the labeled set. It then selects 2.0% images from the rest of the unlabeled set in each cycle until reaching 10.0% of the training set. In each cycle, the model is trained for 26 epochs with the mini-batch size 2 and the learning rate 0.001. After

Training		Sample Selection			mAP (%) on Proportion (%) of Labeled Images								
IUL	IUR	Rand.	Max Unc.	Mean Unc.	5.0	7.5	10.0	12.5	15.0	17.5	20.0	100.0	
		✓			28.31	49.42	56.03	59.81	64.02	65.95	67.09		
✓		✓			30.09	49.17	55.64	60.93	64.10	65.77	67.20	77.28	
✓			✓		30.09	49.79	58.94	63.11	65.61	67.84	69.01		
✓				✓	30.09	49.74	60.60	64.29	67.13	68.76	70.06		
		✓	✓		47.18	57.12	60.68	63.72	66.10	67.59	68.48		
			✓		47.18	57.58	61.74	64.58	66.98	68.79	70.33	78.37	
		✓		✓	47.18	58.03	63.98	66.58	69.57	70.96	72.03		

Table 1. Module ablation on PASCAL VOC. The first line shows the result of the baseline method with random image selection. “Max Unc.” and “Mean Unc.” respectively denote that the image uncertainty is represented by the maximum and averaged instance uncertainty.

20 epochs, the learning rate decreases to 0.0001. The momentum and the weight decay are set to 0.9 and 0.0005 respectively. For SSD, we follow the settings in [40] and [1], where 1k images in PASCAL VOC dataset are selected to initialize the labeled set and 1k images are selected in each cycle. The learning rate is 0.001 for the first 240 epochs and reduced to 0.0001 for the last 60 epochs. The mini-batch size is set to 32 which is required by LL4AL [40].

We compare MIAL with random sampling, entropy sampling, Core-set [30], LL4AL [40] and CDAL [1]. For entropy sampling, we use the averaged instance entropy as the image uncertainty. We repeat all experiments for 5 times and use the mean performance. MIAL and other methods share the same random seed and initialization for a fair comparison. λ defined in Eqs. (2), (4), (8) and (9) is set to 0.5 and k mentioned in Sec. 3.4 is set to 10k.

4.2. Performance

PASCAL VOC. In Fig. 5, we report the performance of MIAL and compare it with state-of-the-art methods. Using either the RetinaNet [19] or SSD [22] detector, MIAL outperforms state-of-the-art methods with large margins. Particularly, it respectively outperforms state-of-the-art methods by 18.08%, 7.78%, and 5.19% when using 5.0%, 7.5%, and 10.0% samples. In the last cycle, with 20.0% samples, MIAL achieves 72.27% detection mAP, which significantly outperforms CDAL by 3.20%. The improvements validate that MIAL can precisely learn instance uncertainty while selecting informative images. When using the SSD detector, MIAL outperforms state-of-the-art methods in almost all cycles, demonstrating the general applicability of MIAL to object detectors.

MS COCO. MS COCO is a challenging dataset for more categories, denser objects, and larger scale variation, where MIAL also outperforms the compared methods, Fig. 5. Particularly, it respectively outperforms Core-set

Training		mAP (%) on Proportion (%) of Labeled Img.				
IUL		2.0	4.0	6.0	8.0	10.0
		51.01	61.48	69.14	75.14	79.77
✓		58.07	67.75	74.91	78.88	80.96

Table 2. The effect of IUL for active image classification. Experiments are conducted on CIFAR-10 using the ResNet-18 backbone while the images are randomly selected in all cycles.

w_i	Set	mAP (%) on Proportion (%) of Labeled Img.						
		5.0	7.5	10.0	12.5	15.0	17.5	20.0
1	\emptyset	30.09	49.17	55.64	60.93	64.10	65.77	67.20
$\hat{y}_i^{f_1}$	\emptyset	31.67	50.67	55.93	60.78	64.17	66.22	67.30
1	\mathcal{X}_L	42.52	54.08	57.18	63.43	65.04	66.74	68.32
$\hat{y}_i^{f_{mil}}$	\mathcal{X}	47.18	57.12	60.68	63.72	66.10	67.59	68.48

Table 3. Ablation study on IUR. “ w_i ” is the w_i in Eq. (7). “Set” denotes the sample set for IUR. \mathcal{X} and \mathcal{X}_L denote the whole sample set and the labeled set, respectively.

and CDAL by 0.6%, 0.5%, and 2.0%, and 0.6%, 1.3%, and 2.6% when using 2.0%, 4.0%, and 10.0% labeled images.

4.3. Ablation Study

IUL. As shown in Tab. 1, with IUL, the detection performance is improved up to 70.06% in the last cycle, which outperforms the Random method by 2.97% (70.06% vs. 67.09%). In Tab. 2, IUL also significantly improves the image classification performance with active learning on CIFAR-10. Particularly when using 2.0% samples, it improves the classification performance by 7.06% (58.07% vs. 51.01%), demonstrating the effectiveness of the discrepancy learning module for instance uncertainty estimation.

λ	k	mAP (%) on Proportion (%) of Labeled Imgs.						
		5.0	7.5	10.0	12.5	15.0	17.5	20.0
2	10k	47.18	56.94	64.44	67.70	69.58	70.67	72.12
1	10k	47.18	57.30	64.93	67.40	69.63	70.53	71.62
0.5	10k	47.18	58.41	64.02	67.72	69.79	71.07	72.27
0.2	10k	47.18	58.02	64.44	67.67	69.42	70.98	72.06
0.5	N	47.18	58.03	63.98	66.58	69.57	70.96	72.03
0.5	10k	47.18	58.41	64.02	67.72	69.79	71.07	72.27
0.5	100	47.18	58.74	63.62	67.03	68.63	70.26	71.47
0.5	1	47.18	57.58	61.74	64.58	66.98	68.79	70.33

Table 4. Performance under different hyper-parameters.

Method	Time (h) on Proportion (%) of Labeled Imgs.						
	5.0	7.5	10.0	12.5	15.0	17.5	20.0
Random	0.77	1.12	1.45	1.78	2.12	2.45	2.78
CDAL [1]	1.18	1.50	1.87	2.19	2.68	2.83	2.82
MIAL	1.03	1.42	1.78	2.18	2.55	2.93	3.12

Table 5. Comparison of time cost on PASCAL VOC.

IUR. In Tab. 1, IUL achieves comparable performance with the Random method using the random image selection strategy in the early cycles. This is because there are significant noisy instances that make the instance uncertainty inconsistent with the image uncertainty. After using IUR to re-weight instance uncertainty, the performance at early cycles is largely improved by 5.04%~17.09% in the first three cycles (row 4 *vs.* row 1 in Tab. 3). In the last cycle, the performance is improved by 1.28% (68.48% *vs.* 67.20%) in comparison with IUL and 1.39% in comparison with the Random method (68.48% *vs.* 67.09%). As shown in Tab. 3, MIL score $\hat{y}_i^{f_{mil}}$ is the best re-weighting metric (row 4 *vs.* others). Interestingly, when using 100.0% images for training, the detector with IUR outperforms the detector without IUR by 1.09% (78.37% *vs.* 77.28%). These results clearly verify that the IUR module can suppress the interfering instances while highlighting more representative ones, which can indicate informative images for detector training.

Parameters and Time Cost. The effects of the regularization factor λ defined in Eqs. (2), (4), (8) and (9) and the valid instance number k in each image for selection are shown in Tab. 4. One can see that we have the best performance when λ is set to 0.5 and k is set to 10k (for \sim 100k instances/anchors in each image). Tab. 5 shows that MIAL costs less time at early cycles and slightly more time at later cycles than CDAL.

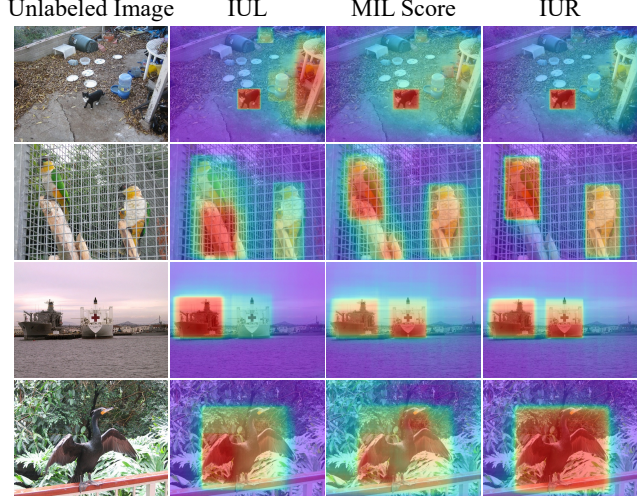


Figure 6. Visualization of learned and re-weighted instance uncertainty and MIL score. (Best viewed in color)

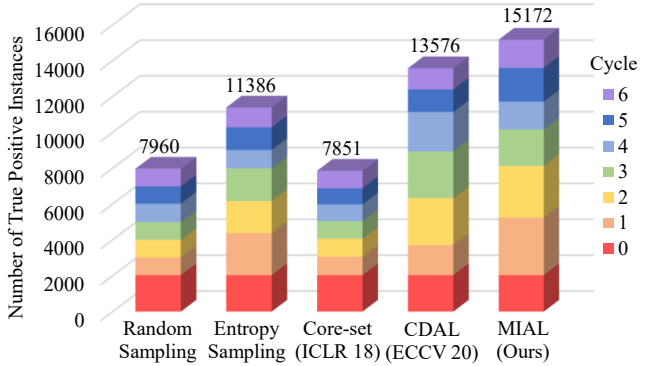


Figure 7. The number of true positive instances selected in each active learning cycle on PASCAL VOC using RetinaNet backbone.

4.4. Model Analysis

Visualization Analysis. In Fig. 6, we visualize the learned and re-weighted uncertainty and MIL scores of instances. The heatmaps are calculated by summarizing the uncertainty scores of all instances. With only IUL, there exist interference instances from the background (row 1) or around the true positive instance (row 2), and the results tend to miss the true positive instances (row 3) or instance parts (row 4). MIL can assign high scores to the instances of interesting while suppressing backgrounds. As a result, IUR leverages the MIL scores to re-weight instances towards accurate instance uncertainty prediction.

Statistical Analysis. In Fig. 7, we calculate the number of true positive instances selected in each active learning cycle. It can be seen that MIAL hits significantly more true positives in all learning cycles. This shows that the proposed MIAL approach can better activate true positive objects while filtering out interfering instances, which facilitates selecting informative images for detector training.

5. Conclusion

We have proposed Multiple Instance Active Learning (MIAL) to select informative images for detector training by observing instance uncertainty. MIAL incorporates a discrepancy learning module, which leverages adversarial instance classifiers to learn the uncertainty of unlabeled instances. MIAL treats the unlabeled images as instance bags and estimates the image uncertainty by re-weighting instances in a multiple instance learning (MIL) fashion. Iterative instance uncertainty learning and instance uncertainty re-weighting facilitate suppressing noisy instances, towards selecting informative images for detector training. Experiments on large-scale datasets have validated the superiority of MIAL, in striking contrast with state-of-the-art methods. MIAL sets a solid baseline for active object detection.

References

- [1] Sharat Agarwal, Himanshu Arora, Saket Anand, and Chetan Arora. Contextual diversity for active learning. In *ECCV*, pages 137–153, 2020. [2](#), [3](#), [7](#), [8](#)
- [2] Hamed Habibi Aghdam, Abel Gonzalez-Garcia, Antonio M. López, and Joost van de Weijer. Active learning for deep detection neural networks. In *ICCV*, pages 3671–3679, 2019. [2](#), [3](#)
- [3] Oisin Mac Aodha, Neill D. F. Campbell, Jan Kautz, and Gabriel J. Brostow. Hierarchical subquery evaluation for active learning on a graph. In *CVPR*, pages 564–571, 2014. [2](#)
- [4] William H. Beluch, Tim Genewein, Andreas Nürnberger, and Jan M. Köhler. The power of ensembles for active learning in image classification. In *CVPR*, pages 9368–9377, 2018. [2](#)
- [5] Hakan Bilen and Andrea Vedaldi. Weakly supervised deep detection networks. In *CVPR*, pages 2846–2854, 2016. [5](#)
- [6] Marc-Andre Carbonneau, Eric Granger, and Ghyslain Gagnon. Bag-level aggregation for multiple-instance active learning in instance classification problems. *IEEE TNNLS*, 30(5):1441–1451, 2019. [2](#)
- [7] Ehsan Elhamifar, Guillermo Sapiro, Allen Y. Yang, and S. Shankar Sastry. A convex optimization framework for active learning. In *ICCV*, pages 209–216, 2013. [2](#)
- [8] Alexander Freytag, Erik Rodner, and Joachim Denzler. Selecting influential examples: Active learning with expected model output changes. In *ECCV*, pages 562–577, 2014. [2](#)
- [9] Yarin Gal, Riashat Islam, and Zoubin Ghahramani. Deep bayesian active learning with image data. In *ICML*, pages 1183–1192, 2017. [2](#)
- [10] Denis A. Gudovskiy, Alec Hodgkinson, Takuya Yamaguchi, and Sotaro Tsukizawa. Deep active learning for biased datasets via fisher kernel self-supervision. In *CVPR*, pages 9038–9046, 2020. [3](#)
- [11] Yuhong Guo. Active instance sampling via matrix partition. In *NeurIPS*, pages 802–810, 2010. [2](#)
- [12] Mahmudul Hasan and Amit K. Roy-Chowdhury. Context aware active learning of activity recognition models. In *ICCV*, pages 4543–4551, 2015. [2](#)
- [13] Sheng-Jun Huang, Nengneng Gao, and Songcan Chen. Multi-instance multi-label active learning. In *IJCAI*, pages 1886–1892, 2017. [2](#)
- [14] Ajay J. Joshi, Fatih Porikli, and Nikolaos Papanikolopoulos. Multi-class active learning for image classification. In *CVPR*, pages 2372–2379, 2009. [2](#)
- [15] Christoph Käding, Erik Rodner, Alexander Freytag, and Joachim Denzler. Active and continuous exploration with deep neural networks and expected model output changes. *arXiv preprint arXiv:1612.06129*, 2016. [2](#)
- [16] David D. Lewis and Jason Catlett. Heterogeneous uncertainty sampling for supervised learning. In *Machine Learning*, pages 148–156, 1994. [2](#)
- [17] David D. Lewis and William A. Gale. A sequential algorithm for training text classifiers. In *SIGIR*, pages 3–12, 1994. [2](#)
- [18] Liang Lin, Keze Wang, Deyu Meng, Wangmeng Zuo, and Lei Zhang. Active self-paced learning for cost-effective and progressive face identification. *IEEE TPAMI*, 40(1):7–19, 2018. [2](#)
- [19] Tsung-Yi Lin, Priya Goyal, Ross B. Girshick, Kaiming He, and Piotr Dollár. Focal loss for dense object detection. *IEEE TPAMI*, 42(2):318–327, 2020. [3](#), [4](#), [6](#), [7](#)
- [20] Binghao Liu, Yao Ding, Jianbin Jiao, Ji Xiangyang, and Qixiang Ye. Anti-aliasing semantic reconstruction for few-shot semantic segmentation. In *CVPR*, 2021. [1](#)
- [21] Binghao Liu, Jianbin Jiao, and Qixiang Ye. Harmonic feature activation for few-shot semantic segmentation. *IEEE TIP*, pages 3142–3153, 2021. [1](#)
- [22] Wei Liu, Dragomir Anguelov, Dumitru Erhan, Christian Szegedy, Scott Reed, Cheng-Yang Fu, and Alexander C Berg. Ssd: Single shot multibox detector. In *ECCV*, pages 21–37, 2016. [7](#)
- [23] Wei Liu, Dragomir Anguelov, Dumitru Erhan, Christian Szegedy, Scott E. Reed, Cheng-Yang Fu, and Alexander C. Berg. SSD: single shot multibox detector. In *ECCV*, pages 21–37, 2016. [6](#)
- [24] Zhao-Yang Liu and Sheng-Jun Huang. Active sampling for open-set classification without initial annotation. In *AAAI*, pages 4416–4423, 2019. [2](#)
- [25] Zhao-Yang Liu, Shao-Yuan Li, Songcan Chen, Yao Hu, and Sheng-Jun Huang. Uncertainty aware graph gaussian process for semi-supervised learning. In *AAAI*, pages 4957–4964, 2020. [2](#)
- [26] Wenjie Luo, Alexander G. Schwing, and Raquel Urtasun. Latent structured active learning. In *NeurIPS*, pages 728–736, 2013. [2](#)
- [27] Hieu Tat Nguyen and Arnold W. M. Smeulders. Active learning using pre-clustering. In *ICML*, 2004. [2](#)
- [28] Dan Roth and Kevin Small. Margin-based active learning for structured output spaces. In *ECML*, pages 413–424, 2006. [2](#)
- [29] Nicholas Roy and Andrew McCallum. Toward optimal active learning through sampling estimation of error reduction. In *ICML*, pages 441–448, 2001. [2](#)

- [30] Ozan Sener and Silvio Savarese. Active learning for convolutional neural networks: A core-set approach. In *ICLR*, 2018. [2](#), [7](#)
- [31] Burr Settles. *Active Learning*. Synthesis Lectures on Artificial Intelligence and Machine Learning. 2012. [2](#)
- [32] Burr Settles and Mark Craven. An analysis of active learning strategies for sequence labeling tasks. In *EMNLP*, pages 1070–1079, 2008. [2](#)
- [33] Burr Settles, Mark Craven, and Soumya Ray. Multiple-instance active learning. In *NeurIPS*, pages 1289–1296, 2007. [2](#)
- [34] Samarth Sinha, Sayna Ebrahimi, and Trevor Darrell. Variational adversarial active learning. In *ICCV*, pages 5971–5980, 2019. [2](#)
- [35] Andrews Stuart, Tsochantaridis Ioannis, and Hofmann Thomas. Support vector machines for multiple-instance learning. In *NeurIPS*, pages 561–568, 2002. [5](#)
- [36] Ying-Peng Tang and Sheng-Jun Huang. Self-paced active learning: Query the right thing at the right time. In *AAAI*, pages 5117–5124, 2019. [2](#)
- [37] Keze Wang, Dongyu Zhang, Ya Li, Ruimao Zhang, and Liang Lin. Cost-effective active learning for deep image classification. *IEEE TCSVT*, 27(12):2591–2600, 2017. [2](#)
- [38] Ran Wang, Xi-Zhao Wang, Sam Kwong, and Chen Xu. Incorporating diversity and informativeness in multiple-instance active learning. *IEEE TFS*, 25(6):1460–1475, 2017. [2](#)
- [39] Yi Yang, Zhigang Ma, Feiping Nie, Xiaojun Chang, and Alexander G. Hauptmann. Multi-class active learning by uncertainty sampling with diversity maximization. *IJCV*, 113(2):113–127, 2015. [2](#)
- [40] Donggeun Yoo and In So Kweon. Learning loss for active learning. In *CVPR*, pages 93–102, 2019. [2](#), [3](#), [7](#)
- [41] Beichen Zhang, Liang Li, Shijie Yang, Shuhui Wang, Zheng-Jun Zha, and Qingming Huang. State-relabeling adversarial active learning. In *CVPR*, pages 8753–8762, 2020. [2](#)